Exact zeros of fidelity in finite-size systems as a signature for probing quantum phase transitions

Yumeng Zeng [1,2] Bozhen Zhou [1] and Shu Chen [1,2,*]

[1]*Beijing National Laboratory for Condensed Matter Physics, Institute of Physics, Chinese Academy of Sciences, Beijing 100190, China*
[2]*School of Physical Sciences, University of Chinese Academy of Sciences, Beijing 100049, China*

The fidelity is widely used to detect quantum phase transitions, which is characterized by either a sharp change of fidelity or the divergence of fidelity susceptibility in the thermodynamical limit when the phase-driving parameter is across the transition point. In this work, we unveil that the occurrence of exact zeros of fidelity in finite-size systems can be applied to detect quantum phase transitions. In general, the fidelity $\mathcal{F}(\gamma, \tilde{\gamma})$ always approaches zero in the thermodynamical limit, due to the Anderson orthogonality catastrophe, no matter whether the parameters of two ground states (γ and $\tilde{\gamma}$) are in the same phase or different phases, and this makes it difficult to distinguish whether an exact zero of fidelity exists by finite-size analysis. To overcome the influence of orthogonality catastrophe, we study finite-size systems with twist boundary conditions, which can be introduced by applying a magnetic flux, and demonstrate that exact zeros of fidelity can be always accessed by tuning the magnetic flux when γ and $\tilde{\gamma}$ belong to different phases. On the other hand, no exact zero of fidelity can be observed if γ and $\tilde{\gamma}$ are in the same phase. We demonstrate the applicability of our theoretical scheme by studying concrete examples, including the Su-Schrieffer-Heeger model, Creutz model, and Haldane model. Our work provides a practicable way to detect quantum phase transitions via the calculation of fidelity of finite-size systems.

I. INTRODUCTION

A quantum phase transition represents qualitative changes in the ground-state properties of quantum systems induced by varying control parameters [1]. These changes become nonanalytic around the phase transition point in the infinite-size limit and can be revealed by the response of physical quantities to changes in phase-driving parameters. The notion of fidelity between two pure ground states has become a well-established method of detection of quantum phase transitions [2–5]. So far, fidelity and fidelity susceptibility have been applied to study phase transitions in various systems [2–18]. Given γ is a phase-driving parameter of the system, the fidelity is defined as the module of the overlap of two ground states, i.e.,

$$\mathcal{F}(\gamma, \tilde{\gamma}) = |\langle \psi^0(\gamma) | \psi^0(\tilde{\gamma}) \rangle|, \qquad (1)$$

where $|\psi^0(\gamma)\rangle$ is the ground state of the Hamiltonian $H(\gamma)$ and $\tilde{\gamma}$ is a parameter value different from γ. If two parameters are very close, i.e., $\delta = \tilde{\gamma} - \gamma$ is a small quantity, then quantum phase transitions are associated with a drop in the fidelity when γ and $\tilde{\gamma}$ are in different phases. Hence the second derivative of the fidelity, called *fidelity susceptibility*, is divergent at the quantum phase transition point in the thermodynamical limit.

The divergence of fidelity susceptibility at quantum phase transition point suggests that $\mathcal{F}(\gamma, \tilde{\gamma})$ may have a different property when γ and $\tilde{\gamma}$ are in different phase regions. Recent studies on dynamical quantum phase transitions [19–28] have unveiled that the Loschmdot echo can have exact zero points at some critical times when the postquench parameter and prequench parameter are in different phase regions [19–21,26–29], whereas it may have no zero point if the postquench parameter and prequench parameter are in the same phase region. Motivated by these results, one may ask whether $\mathcal{F}(\gamma, \tilde{\gamma})$ has (has no) exact zero points when γ and $\tilde{\gamma}$ are in different (the same) phase regions. Although the question seems very natural, it is hard to give a simple answer due to the existence of the Anderson orthogonality catastrophe (OC) in the thermodynamic limit. According to the OC, when the system size increases to infinity, even a slight perturbation leads to a many-body ground state having zero overlap with the slightly perturbed state [30]. Therefore, $\mathcal{F}$ approaches zero in the thermodynamic limit as long as $\tilde{\gamma}$ and γ are not equal, no matter whether $\tilde{\gamma}$ and γ are in the same or different phase regions.

In this work, we unveil that the fidelity exhibits different features for $\tilde{\gamma}$ and γ in the same and different phase regions by studying several typical two-band quantum systems, which display quantum phase transitions. For systems with translation symmetry, the fidelity can be represented as the product of $\mathcal{F}_k$, i.e., $\mathcal{F}(\gamma, \tilde{\gamma}) = \prod_k \mathcal{F}_k(\gamma, \tilde{\gamma})$, where $\mathcal{F}_k(\gamma, \tilde{\gamma})$ is the fidelity of the k mode, which represents the overlap of wave funtions in the momentum space with momentum k and different parameters γ and $\tilde{\gamma}$. Although the fidelity is found to decay exponentially with the increase of L as a result of the OC and thus always approaches zero in the thermodynamical limit, we demonstrate that there exists at least one k_c mode so that $\mathcal{F}_{k_c} = 0$ is fulfilled for $\tilde{\gamma}$ and γ in different

*Contact author: schen@iphy.ac.cn

phases, whereas such a k_c mode is absent for $\tilde{\gamma}$ and γ in the same phase. Under the periodic boundary condition (PBC), the momentum k of a finite-size system can take only some discrete values, which do not cover the whole momentum space continuously. Therefore, usually the k_c mode is only accessible in the thermodynamical limit, and thus the exact zero of the fidelity does not exist in finite-size systems. For the modes k' located in the vicinity of k_c, $\mathcal{F}_{k'}$ approach zero in terms of $\mathcal{F}_{k'} \propto 1/L$ when $\tilde{\gamma}$ and γ are in different phases. Due to the existence of OC, it is hard to distinguish whether the k_c modes exist from the analysis of size-dependent behavior of $\mathcal{F}(\gamma, \tilde{\gamma})$, as $\mathcal{F}(\gamma, \tilde{\gamma})$ always decays exponentially with the increase of L no matter whether γ and $\tilde{\gamma}$ in the same phase or different phases. In order to reduce the impact of OC, we shall fix the lattice size L and introduce a magnetic flux ϕ into the periodic boundary system, so we can shift the momentum k continuously to access k_c by choosing a proper twist boundary condition. In this way, we can always access $\mathcal{F}(\gamma, \tilde{\gamma}) = 0$ by tuning ϕ, when $\tilde{\gamma}$ and γ are in different phase regions, whereas no exact zero of fidelity is accessible for $\tilde{\gamma}$ and γ in the same phase region. Therefore, under a proper twist boundary condition, the fidelity $\mathcal{F}(\gamma, \tilde{\gamma})$ of a finite-size system does not change continuously with $\tilde{\gamma}$ and a discontinuous change from nonzero to zero value occurs at the phase transition point. As a consequence, the discontinuity of the fidelity can be viewed as a signature for detecting quantum phase transition in finite-size systems.

In order to reduce the influence of the system size, it is convenient to introduce a decay rate function defined by

$$\alpha = -\frac{1}{L} \ln \mathcal{F}(\gamma, \tilde{\gamma}). \tag{2}$$

For a finite L, the exact zero of the fidelity means the divergence of α. Therefore, we can observe the divergence of α by tuning ϕ when $\tilde{\gamma}$ and γ are in different phase regions, whereas no divergence of α can be observed for the case with $\tilde{\gamma}$ and γ in the same phase region. This indicates that the emergence of singularity in the decay rate function of a finite-size system via the modulation of ϕ can be used to detect quantum phase transition.

II. MODELS, SCHEME, AND RESULTS

Consider a general two-band system with the Hamiltonian in momentum space described by

$$\hat{h}_k(\gamma) = \sum_{\beta=x,y,z} d_{\beta,k}(\gamma)\hat{\sigma}_\beta + d_{0,k}(\gamma)\hat{\mathbb{I}}, \tag{3}$$

where $\hat{h}_k(\gamma)$ is the Hamiltonian of k mode with momentum k, γ is a phase transition driving parameter, $\hat{\sigma}_\beta$ ($\beta = x, y, z$) are Pauli matrices, $d_{\beta,k}(\gamma)$ and $d_{0,k}(\gamma)$ are the corresponding vector components of $\hat{h}_k(\gamma)$, and $\hat{\mathbb{I}}$ denotes the unit matrix. The fidelity of the system can be represented as

$$\mathcal{F}(\gamma, \tilde{\gamma}) = \prod_k \mathcal{F}_k = \prod_k \left| \langle \psi_k^0(\gamma) | \psi_k^0(\tilde{\gamma}) \rangle \right|, \tag{4}$$

where $|\psi_k^0(\gamma)\rangle$ and $|\psi_k^0(\tilde{\gamma})\rangle$ are the ground state of $\hat{h}_k(\gamma)$ and $\hat{h}_k(\tilde{\gamma})$, respectively. Then we have

$$\mathcal{F}_k = \sqrt{\frac{\sum_\beta d_{\beta,k}(\gamma) d_{\beta,k}(\tilde{\gamma})}{2 E_k \tilde{E}_k} + \frac{1}{2}}, \tag{5}$$

where $E_k = \sqrt{\sum_\beta d_{\beta,k}^2(\gamma)}$ and $\tilde{E}_k = \sqrt{\sum_b et a d_{\beta,k}^2(\tilde{\gamma})}$.

To ensure $\mathcal{F} = 0$, one needs at least one k mode fulfilling $\mathcal{F}_k = 0$, which gives rise to the following four constraint relations:

$$d_{x,k}(\gamma) d_{y,k}(\tilde{\gamma}) = d_{y,k}(\gamma) d_{x,k}(\tilde{\gamma}), \tag{6}$$

$$d_{x,k}(\gamma) d_{z,k}(\tilde{\gamma}) = d_{z,k}(\gamma) d_{x,k}(\tilde{\gamma}), \tag{7}$$

$$d_{y,k}(\gamma) d_{z,k}(\tilde{\gamma}) = d_{z,k}(\gamma) d_{y,k}(\tilde{\gamma}), \tag{8}$$

$$\sum_\beta d_{\beta,k}(\gamma) d_{\beta,k}(\tilde{\gamma}) < 0. \tag{9}$$

The first three equations determine the value of k_c, and the last one determines the phase transition point γ_c. The four formulas should be satisfied simultaneously. It means that $\vec{d}_k(\gamma)$ and $\vec{d}_k(\tilde{\gamma})$ should be antiparallel on the bloch sphere. Note that here $\tilde{\gamma}$ and γ should be in two adjacent phases.

To make our discussion concrete, first we consider the Su-Schrieffer-Heeger (SSH) model as a showcase example and give the details of calculation. Then we generalize our study to the Creutz model and Haldane model.

A. SSH model

The SSH model [31] is described by the Hamiltonian

$$H = \sum_{j=1}^{L} (t_1 c_{j,A}^\dagger c_{j,B} + t_2 c_{j,B}^\dagger c_{j+1,A} + \text{H.c.}), \tag{10}$$

where t_1 and t_2 denote the intracellular and intercellular hopping amplitudes, respectively, and $c_{j,A(B)}^\dagger$ and $c_{j,A(B)}$ are fermionic creation and annihilation operators of the $A(B)$ sublattice on the jth site. By taking a Fourier transformation $c_{j,A(B)}^\dagger = \frac{1}{\sqrt{L}} \sum_k e^{ikj} c_{k,A(B)}^\dagger$, the Hamiltonian in the momentum space can be written as

$$H = \sum_k \psi_k^\dagger \hat{h}_k \psi_k, \tag{11}$$

where $\psi_k = (c_{k,A}, c_{k,B})^T$ and $\hat{h}_k$ takes the form of Eq. (3) with the vector components

$$d_{x,k} = t_1 + t_2 \cos k, \tag{12}$$

$$d_{y,k} = -t_2 \sin k, \tag{13}$$

and $d_{z,k} = d_{0,k} = 0$. The SSH model possesses two topologically different phases for $t_2 > t_1$ and $t_2 < t_1$ with a phase transition point at $t_{2c}/t_1 = 1$ [32]. Setting $\gamma = t_2/t_1$, the
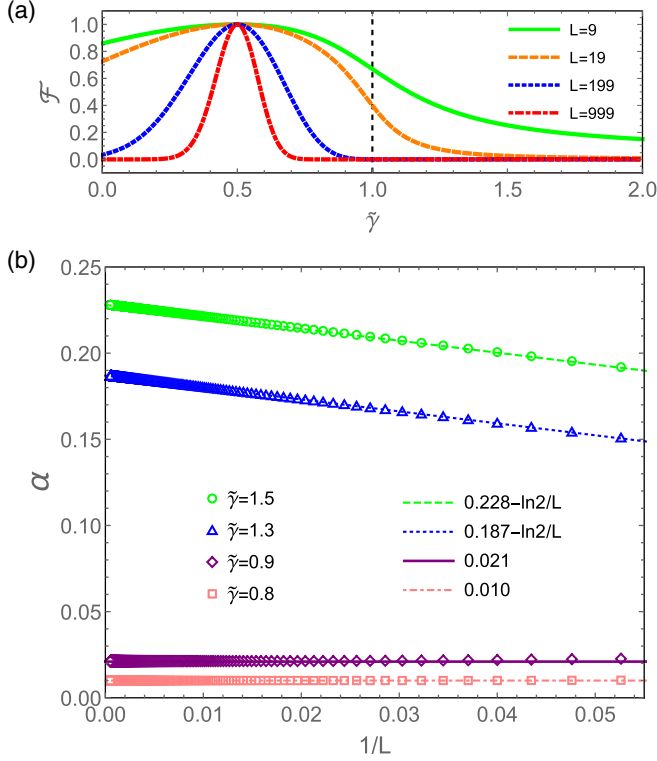
FIG. 1. (a) The fidelity $\mathcal{F}$ of the SSH model versus $\tilde{\gamma}$ for different system sizes $L = 9, 19, 199$, and 999. The vertical dashed line guides the critical point $\tilde{\gamma}_c = 1$. (b) The image of α versus $1/L$. The pink squares, purple diamonds, blue triangles, and green circles denote results for $\tilde{\gamma} = 0.8, 0.9, 1.3$, and 1.5, respectively. The dot-dashed pink, solid purple, dotted blue, and dashed green lines represent the corresponding fitting lines. Here we take $\gamma = 0.5$ and use the periodic boundary condition.

fidelity of the SSH model is

$$\mathcal{F}_k = \sqrt{\frac{1 + (\gamma + \tilde{\gamma})\cos k + \gamma\tilde{\gamma}}{2\sqrt{(1 + 2\gamma\cos k + \gamma^2)(1 + 2\tilde{\gamma}\cos k + \tilde{\gamma}^2)}} + \frac{1}{2}}. \tag{14}$$

According to Eqs. (6)–(9), the constraint relations for the occurrence of exact zeros of $\mathcal{F}$ are

$$(\gamma + 1)(\tilde{\gamma} + 1) < 0, k_c = 0;$$
$$(\gamma - 1)(\tilde{\gamma} - 1) < 0, k_c = \pi. \tag{15}$$

For a finite-size system under the PBC, the momentum k takes discrete values $k = 2\pi m/L$ with $m = -L/2 + 1, -L/2 + 2, \ldots, L/2$ if L is even or $m = -(L-1)/2, -(L-1)/2 + 1, \ldots, (L-1)/2$ if L is odd. For the case of $\gamma > 0$ and $\tilde{\gamma} > 0$, if $\gamma < 1$, then Eq. (15) is fulfilled only for $\tilde{\gamma} > 1$; if $\gamma > 1$, then Eq. (15) is fulfilled only for $\tilde{\gamma} < 1$. It means that $\mathcal{F} = 0$ happens only when γ and $\tilde{\gamma}$ are in different topological phases which are separated by the phase transition point $\gamma_c = 1$ and the corresponding k mode is $k_c = \pi$.

Now we consider the case with odd size L under PBC. The momentum k enforced by the PBC can take the value of $k = \pi(1 - 1/L)$, which approaches $k_c = \pi$ in the limit of $L \to \infty$. In Fig. 1(a), we display $\mathcal{F}$ versus $\tilde{\gamma}$ by fixing $\gamma = 0.5$ for various L. It shows that $\mathcal{F}$ is finite for small odd sizes and
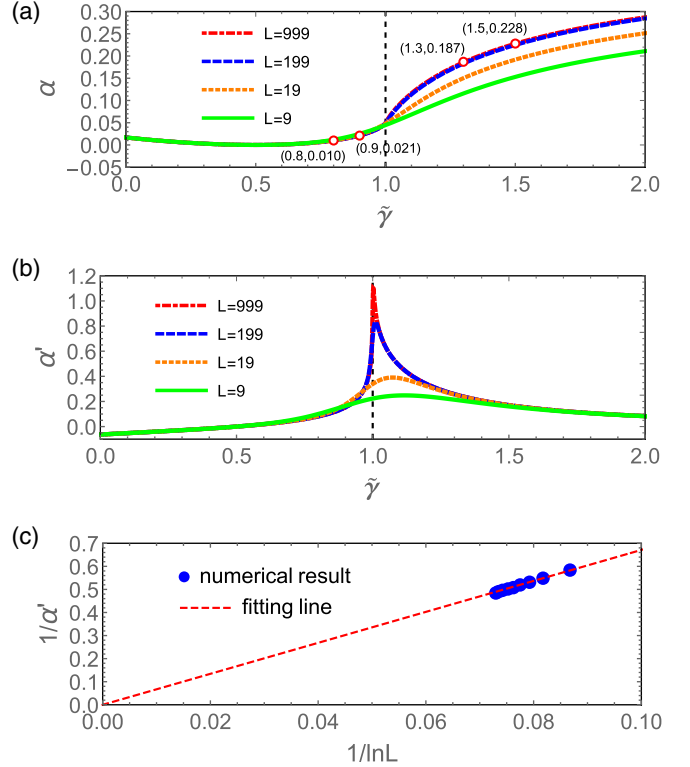
FIG. 2. (a) The images of α versus $\tilde{\gamma}$ for the SSH model with different system sizes $L = 9, 19, 199$, and 999. The four red circles denote values of α in the thermodynamical limit obtained from finite-size analysis for $\tilde{\gamma} = 0.8, 0.9, 1.3$, and 1.5, respectively. (b) The images of the derivative of α versus $\tilde{\gamma}$ for the SSH model with different system sizes $L = 9, 19, 199$, and 999. The vertical dashed line guides the critical point $\tilde{\gamma}_c = 1$. (c) The image of the inverse of the derivative of α versus $1/\ln L$ for $\tilde{\gamma} = 1$. The blue points are numerical result of $L \in [100000, 1000000]$. The red dashed line is a fitting line. Here we take $\gamma = 0.5$ and use the periodic boundary condition.

approaches zero with the increase of L for $\tilde{\gamma}$ and γ either in the same phase or different phases. In Fig. 1(b), we plot the image of α versus $1/L$. While α is constant for $\tilde{\gamma}$ and γ in the same phase, α versus $1/L$ can be well fitted by an oblique line with the slope $-\ln 2$ for $\tilde{\gamma}$ and γ in different phases, i.e., the fitting curves for $\tilde{\gamma}$ and γ in the same or different phase are described by $-\frac{1}{L}\ln\mathcal{F} = c$ or $-\frac{1}{L}\ln\mathcal{F} = c - \frac{1}{L}\ln 2$, respectively, where c represents a constant. The additional term of $-\frac{1}{L}\ln 2$ is originated from the existence of the k_c mode ($\mathcal{F}_{k_c} = 0$) [33].

In Fig. 2(a), we plot α versus $\tilde{\gamma}$ for the SSH model with fixed $\gamma = 0.5$ and different system sizes $L = 9, 19, 199$, and 999. For $\tilde{\gamma}$ and γ in the same phase, α is almost the same for different sizes. For $\tilde{\gamma}$ and γ in different phases, the value of α goes up and tends to a fixed value with the increase of L, which is in accordance with the result of Fig. 1(b). Given $\gamma = 0.5$, for the case of $\tilde{\gamma} < 1$, $\mathcal{F} \to 0$ in the limit of $L \to \infty$ is purely caused by the OC. However, for the case of $\tilde{\gamma} > 1$, besides the OC, k_c can be approached in terms of $\min|k - k_c| = \pi/L$, thus $\mathcal{F}_{k_c} = 0$ is achievable in the thermodynamical limit of $L \to \infty$. In contrast, no k mode fulfills $\mathcal{F}_k = 0$ for the case of $\tilde{\gamma} < 1$. The different scaling behaviors of the decay rate

function α in the regions of $\tilde{\gamma} < 1$ and $\tilde{\gamma} > 1$ are due to the absence and presence of the k_c mode in these regions.

To explore the nonanalytical behavior of $\alpha(\tilde{\gamma})$ at the critical point, we calculate the derivative of $\alpha(\tilde{\gamma})$ with respect to $\tilde{\gamma}$ via

$$\alpha'(\tilde{\gamma}) = -\frac{1}{2L} \sum_k \left[\frac{E_k \tilde{E}_k' + \sum_\beta d_{\beta,k}(\gamma) d_{\beta,k}'(\tilde{\gamma})}{E_k \tilde{E}_k + \sum_\beta d_{\beta,k}(\gamma) d_{\beta,k}(\tilde{\gamma})} - \frac{\tilde{E}_k'}{\tilde{E}_k} \right]. \tag{16}$$

Here $\tilde{E}_k'$ and $d_{\beta,k}'(\tilde{\gamma})$ are derivatives of $\tilde{E}_k$ and $d_{\beta,k}(\tilde{\gamma})$ with respect to $\tilde{\gamma}$, respectively. In Fig. 2(b), we plot α' versus $\tilde{\gamma}$ for the SSH model with different system sizes $L = 9, 19, 199$, and 999. Figure 2(c) is the result of finite-size-scaling analysis of α' for $\gamma = 0.5$ and $\tilde{\gamma} = 1$. It shows that α' gradually diverges at the critical point $\gamma_c = 1$ as L increases. Therefore, α is non-analytic at the critical point $\gamma_c = 1$ in the thermodynamical limit.

Next we unveil that $\mathcal{F} = 0$ can be realized even in a finite-size system for $\tilde{\gamma}$ and γ in different phases if we introduce a magnetic flux ϕ into the system. The effect of the magnetic flux is equivalent to the introduction of a twist boundary condition in real space $c_{L+1,A(B)}^\dagger = c_{1,A(B)}^\dagger e^{i\phi} [\phi \in (0, 2\pi)]$. Under the twist boundary condition, the quantized momentum $k = \frac{2\pi m + \phi}{L}$ is shifted by a factor ϕ/L, where $m = -L/2 + 1, -L/2 + 2, \ldots, L/2$ for an even L or $m = -(L-1)/2, -(L-1)/2 + 1, \ldots, (L-1)/2$ for an odd L. Therefore, for an odd L we can always achieve k_c by tuning the flux ϕ to $\phi_c = \pi$. Let $\Delta = |\phi_c - \phi|$, we can get

$$\alpha = -\frac{1}{L} \left(\ln \mathcal{F}_{k^*} + \sum_{k \neq k^*} \ln \mathcal{F}_k \right), \tag{17}$$

where $\mathcal{F}_{k^*}$ is the k^* mode which is closest to k_c, i.e., $|k^* - k_c| = \Delta/L$. Let $\Delta \to 0$, we can get

$$\mathcal{F}_{k^*} \approx \frac{|\tilde{\gamma} - \gamma|}{2(\tilde{\gamma} - 1)(1 - \gamma)L} \Delta. \tag{18}$$

When $\Delta \to 0$, $\mathcal{F}_{k^*} \to 0$ and thus $\ln \mathcal{F}_{k^*}$ is divergent, i.e., when ϕ achieves ϕ_c, α becomes divergent.

In Fig. 3(a), we plot the fidelity $\mathcal{F}$ of the SSH model versus $\tilde{\gamma}$ for different boundary conditions $\phi = 0, 0.9\pi$, and π with $\gamma = 0.5$ and $L = 9$. It is evident that $\mathcal{F}$ immediately equals zero when $\tilde{\gamma}$ is across the critical point $\gamma_c = 1$ for $\phi = \pi$, while $\mathcal{F}$ stays nonzero for other ϕ. The existence of the exact zero of $\mathcal{F}$ for a finite odd size system means that the ground state of one phase can be orthogonal to the ground state of the other phase by tuning the magnetic flux. At the same time, $\mathcal{F}_{k_c} = 0$ leads to the divergency of α for a finite L. For a given $\tilde{\gamma}$ and γ, tuning ϕ from 0 to 2π, from Fig. 3(b) we can see that if $\tilde{\gamma}$ and γ belong to the same phase, then the value of α is always small for any value of ϕ, indicating the absence of the exact zero of the fidelity; if $\tilde{\gamma}$ and γ belong to different phases, then α is divergent at $\phi_c/\pi = 1$, which gives a signal of quantum phase transition. As a consequence, we can judge whether a quantum phase transition exists by observing the change of α of a finite system as a function of $\tilde{\gamma}$ and ϕ.
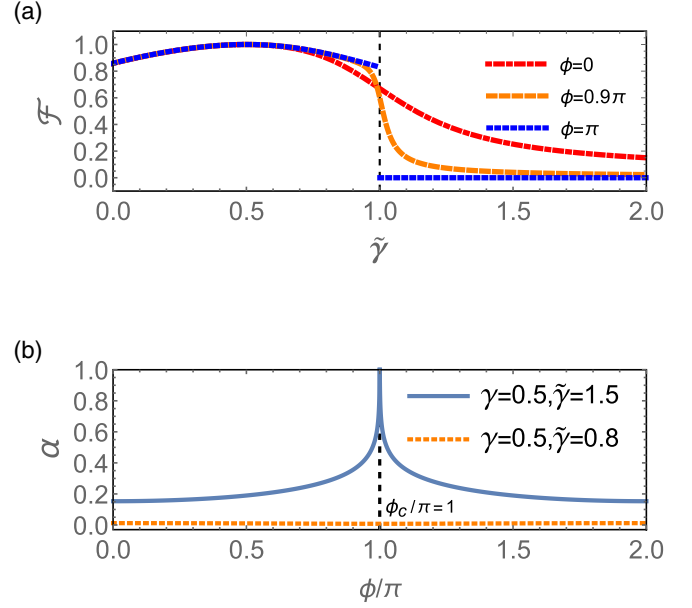

FIG. 3. (a) The fidelity $\mathcal{F}$ of the SSH model versus $\tilde{\gamma}$ under twist boundary conditions with flux parameter $\phi = 0, 0.9\pi$, and π. The vertical dashed line guides the critical point $\tilde{\gamma}_c = 1$. Here $\gamma = 0.5$. (b) The images of α versus ϕ/π. The solid blue line corresponds to $\gamma = 0.5$ and $\tilde{\gamma} = 1.5$, while the dotted orange line corresponds to $\gamma = 0.5$ and $\tilde{\gamma} = 0.8$. The vertical dashed line guides the divergent point $\phi_c/\pi = 1$. Here we take $L = 9$.

B. Creutz model

Next we consider the Creutz model [34,35] described by the Hamiltonian:

$$H = -\sum_{j=1}^L \left[J_h \left(e^{i\theta} c_{j+1}^{p\dagger} c_j^p + e^{-i\theta} c_{j+1}^{q\dagger} c_j^q \right) \right.$$
$$\left. + J_d \left(c_{j+1}^{p\dagger} c_j^q + c_{j+1}^{q\dagger} c_j^p \right) + J_v c_j^{q\dagger} c_j^p + \text{H.c.} \right]. \tag{19}$$

The model describes the dynamics of a spinless electron moving in a ladder system with $c_j^{p(q)\dagger}$ and $c_j^{p(q)}$ denoting fermionic creation and annihilation operators on the jth site of the lower (upper) chain. J_h, J_d, and J_v are coupling strength for horizontal, diagonal, and vertical bonds, respectively, and $\theta \in [-\pi/2, \pi/2]$ denotes the magnetic flux per plaquette induced by a magnetic field piercing the ladder. After a Fourier transformation, the Hamiltonian in the momentum space can be expressed as $H = \sum_k \psi_k^\dagger \hat{h}_k \psi_k$ with $\psi_k = (c_k^q, c_k^p)^T$. The vector components of the Hamiltonian in momentum space are given by

$$d_{x,k} = -2J_d \cos k - J_v, \tag{20}$$

$$d_{z,k} = -2J_h \sin k \sin \theta, \tag{21}$$

$$d_{0,k} = -2J_h \cos k \cos \theta, \tag{22}$$

and $d_{y,k} = 0$. For simplicity, we focus on the case of $J_h = J_d = J$ and $J_v/2J < 1$ and take $J = 1$ as the energy unit. It is known that the Creutz model has two distinct topologically nontrivial phases for $-\pi/2 \leqslant \theta < 0$ and $0 < \theta \leqslant \pi/2$ with a phase transition occurring at $\theta_c = 0$.
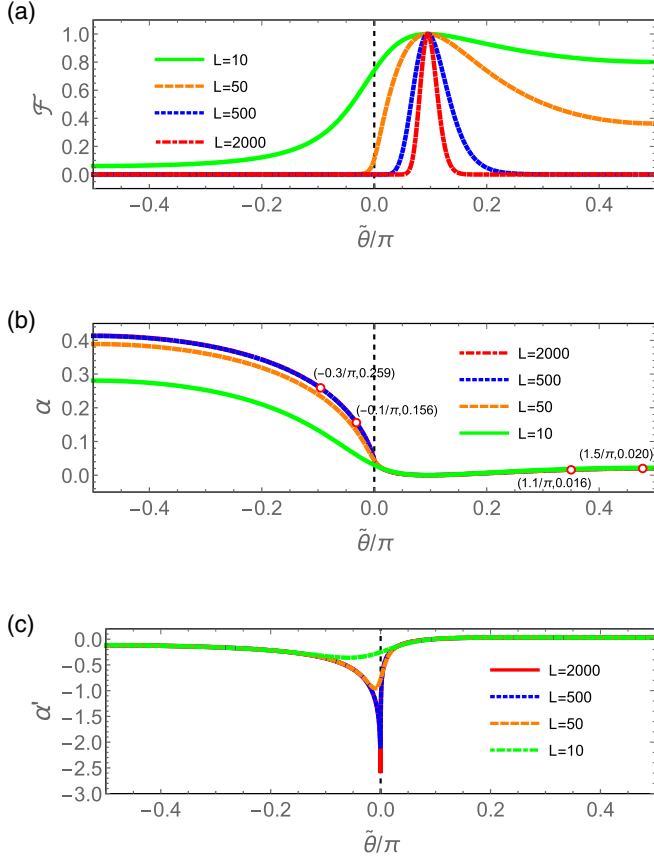
(a)

(b)

(c)

FIG. 4. (a) The fidelity $\mathcal{F}$ of the Creutz model versus $\tilde{\theta}/\pi$ for different system sizes $L = 10, 50, 500$, and 2000. The vertical dashed line guides the critical point $\tilde{\theta}_c = 0$. (b) The images of α versus $\tilde{\theta}/\pi$ for the Creutz model with different system sizes $L = 10, 50, 500$, and 2000. The four red circles denote value of α in the thermodynamical limit obtained from finite-size analysis for $\tilde{\theta} = -0.3, -0.1, 1.1$, and 1.5, respectively. (c) The images of the derivative of α versus $\tilde{\theta}/\pi$ for the Creutz model with different system sizes $L = 10, 50, 500$, and 2000. The vertical dashed line guides the critical point $\tilde{\theta}_c = 0$. Here we take $\theta = 0.3$ and $J_v/(2J) = 0.6$, and use the periodic boundary condition.

The fidelity of the Creutz model is given by

$$\mathcal{F} = \prod_k \sqrt{\frac{[\cos k + J_v/(2J)]^2 + \sin^2 k \sin\theta \sin\tilde{\theta}}{2\epsilon_k \tilde{\epsilon}_k} + \frac{1}{2}}, \quad (23)$$

where $\epsilon_k = \sqrt{[\cos k + J_v/(2J)]^2 + \sin^2 k \sin^2\theta}$ and $\tilde{\epsilon}_k = \sqrt{[\cos k + J_v/(2J)]^2 + \sin^2 k \sin^2\tilde{\theta}}$. We notice that the constraint relations for ensuring $\mathcal{F} = 0$ are

$$\sin\theta \sin\tilde{\theta} < 0, \quad k_{c,\pm} = \pm\arccos[-J_v/(2J)]. \quad (24)$$

If $\theta < 0$, then Eq. (24) is fulfilled only for $\tilde{\theta} > 0$. On the other hand, if $\theta > 0$, then Eq. (24) is fulfilled only for $\tilde{\theta} < 0$. It means that the exact zeros of the fidelity exist only when parameters $\tilde{\theta}$ and θ are across the underlying phase transition point and the corresponding k mode is $k_{c,\pm} = \pm\arccos[-J_v/(2J)]$.

It is clear that $k_{c,\pm}$ are usually not equal to the quantized momentum values $k = 2\pi m/L$ enforced by the PBC. This
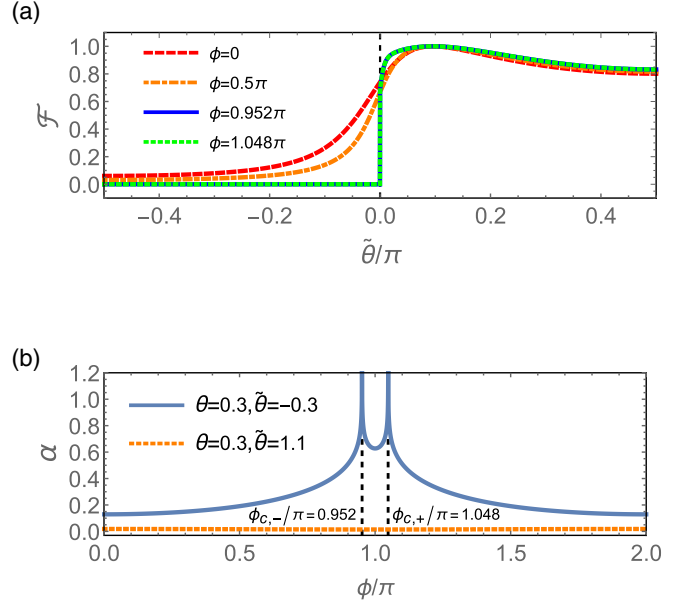
(a)

(b)

FIG. 5. (a) The fidelity $\mathcal{F}$ of the Creutz model versus $\tilde{\theta}/\pi$ under twist boundary conditions with $\phi = 0, 0.5\pi, 0.952\pi$, and 1.048π. The solid blue line and the dotted green line have the same image and therefore overlap each other. The vertical dashed line guides the critical point $\tilde{\theta}_c = 0$. Here $\theta = 0.3$. (b) The images of α versus ϕ/π. The solid blue line corresponds to $\theta = 0.3$ and $\tilde{\theta} = -0.3$, while the dotted orange line corresponds to $\theta = 0.3$ and $\tilde{\theta} = 1.1$. The vertical dashed lines guides the divergent points $\phi_{c,-}/\pi \approx 0.952$ and $\phi_{c,+}/\pi \approx 1.048$. Here we take $J_v/(2J) = 0.6$ and $L = 10$.

means that the exact zeros of $\mathcal{F}$ of a finite-size system generally do not exist for arbitrary $\tilde{\theta}$ and θ. As shown in Fig. 4(a), the fidelity $\mathcal{F}$ is not equal to zero for $L = 10$ but approaches zero with the increase of L as long as $\tilde{\theta} \neq \theta$. Figure 4(b) displays the images of α versus $\tilde{\theta}$ for the Creutz model with different system sizes $L = 10, 50, 500$, and 2000. For $\tilde{\theta}$ and θ in the same phase, α is almost the same for different sizes. For $\tilde{\theta}$ and θ in different phases, since it has two k_c modes $\mathcal{F}_{k_{c,+}}$ and $\mathcal{F}_{k_{c,-}}$, the value of α changes and tends to a fixed value at a rate of $2\ln 2/L$ as the system size increases. Figure 4(c) demonstrates that α' is divergent at the phase transition point $\theta_c = 0$ in the thermodynamical limit of $L \to \infty$.

For a finite-size system under PBC, $k_{c,\pm}$ is usually not achievable. Nonetheless, with the increase in the system size, $k_{c,\pm}$ can be approached in terms of $\min|k - k_{c,\pm}| \leqslant \pi/L$, and thus the exact zeros of $\mathcal{F}$ can be achieved in the limit of $L \to \infty$. Since the quantized momenta k usually do not include $k_{c,\pm}$ under the PBC, we introduce the twist boundary condition $c_{L+1}^{p(q)\dagger} = c_1^{p(q)\dagger} e^{i\phi}[\phi \in (0, 2\pi)]$ here. For a system with a given finite size L, we can always achieve $k_{c,+}$ or $k_{c,-}$ by using the twist boundary condition with

$$\phi_{c,+} = \mathrm{mod}[Lk_{c,+}, 2\pi] \quad \text{or} \quad \phi_{c,-} = \mathrm{mod}[Lk_{c,-}, 2\pi]. \quad (25)$$

For $J_v/(2J) = 0.6$ and $L = 10$, it is easy to get $k_{c,\pm} = \pm 0.705\pi$, $\phi_{c,+} \approx 1.048\pi$ and $\phi_{c,-} \approx 0.952\pi$ from Eqs. (24) and (25).
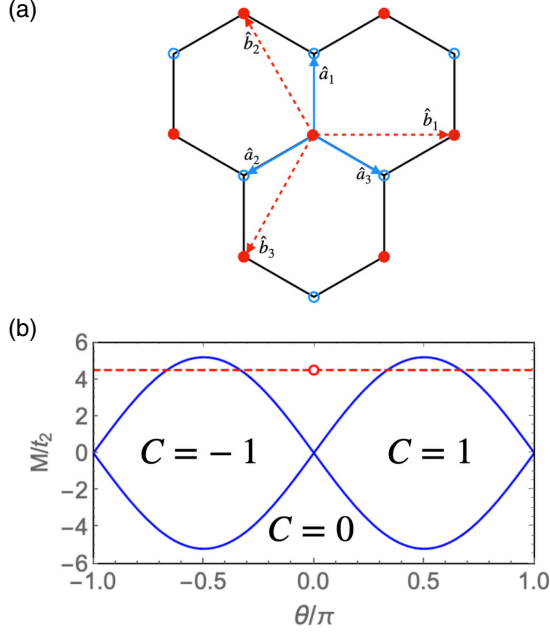
FIG. 6. (a) The illustration of the Haldane model. (b) The phase diagram of the Haldane model. The solid blue lines represent the critical lines. The dashed red line represents parameters at $M/t_2 = 4.5$. The red circle denotes the point $(\theta/\pi, M/t_2) = (0, 4.5)$. Here we take $t_1 = 1$.

Let $\Delta = |\phi - \phi_{c,\pm}|$, we can get

$$\alpha = -\frac{1}{L}\left(\ln \mathcal{F}_{k^*} + \sum_{k \neq k^*} \ln \mathcal{F}_k\right), \tag{26}$$

where $\mathcal{F}_{k^*}$ comes from the contribution of the k^* mode which is closest to $k_{c,\pm}$, i.e., $|k^* - k_{c,\pm}| = \Delta/L$. Let $\Delta \to 0$, and we can get

$$\mathcal{F}_{k^*} \approx -\frac{|\sin\theta - \sin\tilde{\theta}|}{2\sin\theta \sin\tilde{\theta}L}\Delta. \tag{27}$$

This means when $\Delta \to 0$, i.e., $\phi \to \phi_c$, $\mathcal{F}_{k^*} \propto \Delta$. When ϕ reaches $\phi_{c,\pm}$, we can get a k^* mode which satisfies $k^* = k_{c,\pm}$ and $\mathcal{F}_{k^*} = 0$, and thus α becomes divergent.

In Fig. 5(a), we show the fidelity $\mathcal{F}$ of the Creutz model versus $\tilde{\theta}$ for different boundary conditions $\phi = 0$, 0.5π, 0.952π, and 1.048π with $\theta = 0.3$, $J_v/(2J) = 0.6$, and $L = 10$. It demonstrates that $\mathcal{F}$ becomes 0 for $\tilde{\theta} < 0$ when ϕ is tuned to the critical value $\phi_{c,-} \approx 0.952\pi$ and $\phi_{c,+} \approx 1.048\pi$. For a pair of given $\tilde{\theta}$ and θ, Fig. 5(b) exhibits that if $\tilde{\theta}$ and θ belong to the same phase, then α barely changes with ϕ, which means the absence of QPT; if $\tilde{\theta}$ and θ belong to different phases, then α diverges at $\phi_{c,-} \approx 0.952\pi$ and $\phi_{c,+} \approx 1.048\pi$, indicating the occurrence of QPT.

C. Haldane model

The Haldane model is schematically depicted in Fig. 6(a). The red points and blue circles denote A and B sublattice

sites, respectively. The displacements are $\hat{a}_1 = (0, 1)$, $\hat{a}_2 = (-\frac{\sqrt{3}}{2}, -\frac{1}{2})$, $\hat{a}_3 = (\frac{\sqrt{3}}{2}, -\frac{1}{2})$, $\hat{b}_1 = (\sqrt{3}, 0)$, $\hat{b}_2 = (-\frac{\sqrt{3}}{2}, \frac{3}{2})$, and $\hat{b}_3 = (-\frac{\sqrt{3}}{2}, -\frac{3}{2})$. The Hamiltonian of the Haldane model in the real space is described as

$$\begin{aligned} H = & t_1 \sum_{\langle i,j \rangle} (c_{A,\vec{r}_i}^\dagger c_{B,\vec{r}_j} + \text{H.c.}) \\ & + t_2 \sum_{\langle\langle i,j \rangle\rangle} \left(e^{-i\theta}c_{A,\vec{r}_i}^\dagger c_{A,\vec{r}_j} + e^{i\theta}c_{B,\vec{r}_i}^\dagger c_{B,\vec{r}_j} + \text{H.c.}\right) \\ & + M \sum_j \left(c_{A,\vec{r}_j}^\dagger c_{A,\vec{r}_j} - c_{B,\vec{r}_j}^\dagger c_{B,\vec{r}_j}\right). \end{aligned} \tag{28}$$

Here $c_{A(B),\vec{r}_j}^\dagger$ and $c_{A(B),\vec{r}_j}$ denote fermionic creation and annihilation operators of $A(B)$ sublattice on the position $\vec{r}_j$, M $(-M)$ is the on-site potential on $A(B)$ sublattice sites, symbols $\langle i, j \rangle$ and $\langle\langle i, j \rangle\rangle$ denote nearest-neighbor (NN) and next-nearest-neighbor (NNN) hoppings, θ is the additional effective phase of hopping between NNN sites, and t_1 and t_2 are amplitudes of NN hopping and NNN hopping, respectively. Taking the periodic boundary condition along the x axis and y axis and using the Fourier transformation, the Hamiltonian of the Haldane model in the momentum space can be expressed as $H = \sum_{\mathbf{k}} \psi_{\mathbf{k}}^\dagger \hat{h}_{\mathbf{k}} \psi_{\mathbf{k}}$, where $\psi_{\mathbf{k}} = (c_{\mathbf{k},A}, c_{\mathbf{k},B})^T$ and $\hat{h}_{\mathbf{k}}$ is given by [36]

$$\begin{aligned} \hat{h}_{\mathbf{k}} = & 2t_2 \cos\theta \sum_i \cos(\mathbf{k} \cdot \hat{b}_i)I \\ & + t_1 \sum_i \cos(\mathbf{k} \cdot \hat{a}_i)\sigma_x + t_1 \sum_i \sin(\mathbf{k} \cdot \hat{a}_i)\sigma_y \\ & + [M - 2t_2 \sin\theta \sum_i \sin(\mathbf{k} \cdot \hat{b}_i)]\sigma_z, \end{aligned} \tag{29}$$

where $i = 1, 2, 3$ and $\mathbf{k} = (k_x, k_y)$ with $k_x = \frac{2\pi m_x}{\sqrt{3}L_x}$ ($m_x = 1, 2, \ldots, L_x$) and $k_y = \frac{4\pi m_y}{3L_y}$ ($m_y = 1, 2, \ldots, L_y$). It is easy to get

$$d_{x,\mathbf{k}} = t_1\left(\cos k_y + 2\cos\frac{\sqrt{3}k_x}{2}\cos\frac{k_y}{2}\right),$$

$$d_{y,\mathbf{k}} = t_1\left(\sin k_y - 2\cos\frac{\sqrt{3}k_x}{2}\sin\frac{k_y}{2}\right),$$

$$d_{z,\mathbf{k}} = M - 2t_2 \sin\theta\left(\sin\sqrt{3}k_x - 2\sin\frac{\sqrt{3}k_x}{2}\cos\frac{3k_y}{2}\right),$$

and

$$d_{0,\mathbf{k}} = 2t_2 \cos\theta\left(\cos\sqrt{3}k_x + 2\cos\frac{\sqrt{3}}{2}k_x\cos\frac{3}{2}k_y\right).$$

Figure 6(b) shows the phase diagram of the Haldane model. The critical lines of the Haldane model are described by $M/t_2 = \pm 3\sqrt{3}\sin\theta$, which separate topologically different phases characterized by the Chern number with $C = 0$ or $C = \pm 1$ [36]. The corresponding constraint relations for the

occurrence of zeros of fidelity are

$$(M/t_2 + 3\sqrt{3}\sin\theta)(M/t_2 + 3\sqrt{3}\sin\tilde{\theta}) < 0, \quad k_{xc} = \frac{4\pi}{3\sqrt{3}}, \quad k_{yc} = \frac{4\pi}{3};$$

$$(M/t_2 - 3\sqrt{3}\sin\theta)(M/t_2 - 3\sqrt{3}\sin\tilde{\theta}) < 0, \quad k_{xc} = \frac{2\pi}{3\sqrt{3}}, \quad k_{yc} = \frac{2\pi}{3}. \tag{30}$$

According to the above constraint relation, if we choose $\theta = 0$, $t_1 = 1$, $M/t_2 = 4.5$, then zeros of fidelity can be accessible in the thermodynamic limit for $\tilde{\theta} \in (-2\pi/3, -\pi/3) \cup (\pi/3, 2\pi/3)$, which is in accordance with the red dashed line in Fig. 6(b). Next we consider the finite-size system. For $\tilde{\theta} \in (-2\pi/3, -\pi/3)$, $k_{yc} = \frac{4\pi}{3}$ is always accessible. For $\tilde{\theta} \in (\pi/3, 2\pi/3)$, $k_{yc} = \frac{2\pi}{3}$ is accessible for even L_y, while a twist boundary condition $c^{\dagger}_{A(B),\vec{r}_j+L_y(\hat{b}_2-\hat{b}_3)/2} = c^{\dagger}_{A(B),\vec{r}_j}e^{i\phi_y}$ along the y direction is needed such that $k_y = \frac{2(2\pi m_y + \phi_{yc})}{3L_y}$ with $\phi_{yc} = \pi$ can give rise to $k_{yc} = \frac{2\pi}{3}$ for odd L_y. For simplicity, we choose $L_y = 2n$ (even), so that k_{yc} is accessible with no need of the introduction of the twist boundary condition along the y direction.

By applying the twist boundary condition $c^{\dagger}_{A(B),\vec{r}_j+L_x\hat{b}_1} = c^{\dagger}_{A(B),\vec{r}_j}e^{i\phi_x}$ along the x direction, we demonstrate that exact zeros of $\mathcal{F}$ can be accessible by tuning the twist flux ϕ_x when $\tilde{\theta} \in (-2\pi/3, -\pi/3) \cup (\pi/3, 2\pi/3)$. In Fig. 7(a), we show the images of the fidelity $\mathcal{F}$ of the Haldane model versus $\tilde{\theta}$ for systems with different twist flux, where $\theta = 0$, $t_1 = 1$, $M/t_2 = 4.5$, $L_x = 4$, and $L_y = 4$. It is shown that $\mathcal{F}$ drops to zero abruptly at the points $\tilde{\theta} = -2\pi/3$ and $\tilde{\theta} = -\pi/3$ for $\phi_x = 4\pi/3$ and at the points $\tilde{\theta} = \pi/3$ and $\tilde{\theta} = 2\pi/3$ for $\phi_x = 2\pi/3$, while the fidelity for other ϕ_x is analytic everywhere. Under the twist boundary condition, the momentum k_x is shifted and we have $\mathbf{k} = (k_x = \frac{2\pi m_x + \phi_x}{\sqrt{3}L_x}, k_y = \frac{4\pi m_y}{3L_y})$. For $\tilde{\theta} \in (\pi/3, 2\pi/3)$, the $\mathbf{k}_c$ mode can be accessed by tuning the twist flux to $\phi_{xc,1} = 2\pi/3$, whereas for $\tilde{\theta} \in (-2\pi/3, -\pi/3)$, the $\mathbf{k}_c$ mode can be accessed by tuning the twist flux to $\phi_{xc,2} = 4\pi/3$. Actually, for all cases of $L_x = 3n + 1$ with n being a positive integer, we have $\phi_{xc,1} = 2\pi/3$ for $\tilde{\theta} \in (\pi/3, 2\pi/3)$ and $\phi_{xc,2} = 4\pi/3$ for $\tilde{\theta} \in (-2\pi/3, -\pi/3)$. For cases with $L_x = 3n$, we have $\phi_{xc} = 0$. For cases with $L_x = 3n + 2$, we have $\phi_{xc,1} = 4\pi/3$ for $\tilde{\theta} \in (\pi/3, 2\pi/3)$ and $\phi_{xc,2} = 2\pi/3$ for $\tilde{\theta} \in (-2\pi/3, -\pi/3)$. To see it clearly, we show the case of $L_x = 6$ and $L_x = 8$ in Figs. 7(b) and 7(c), respectively. Although the value of ϕ_{xc} may depend on the size of the system, it is clear that the exact zero of the fidelity can be always accessed by continuously tuning the twist flux ϕ_x as long as $\tilde{\theta}$ and θ are in different phase regions.

D. Interacting SSH model

To exhibit the applicability of our theoretical scheme, here we study one more example by taking into account interaction. We shall explore the fidelity of the SSH model with interaction. The Hamiltonian of the interacting SSH model is

$$H = \sum_{j=1}^{L}(c^{\dagger}_{j,A}c_{j,B} + \gamma c^{\dagger}_{j,B}c_{j+1,A} + \text{H.c.})$$

$$+ U\sum_{j=1}^{L}(n_{j,A}n_{j,B} + n_{j,B}n_{j+1,A}), \tag{31}$$

where U is the magnitude of the interaction strength between fermions on nearest-neighboring sites and $n_{j,A(B)} = c^{\dagger}_{j,A(B)}c_{j,A(B)}$. Here we only consider the half-filling case. Reference [37] has analyzed topological phase transitions in
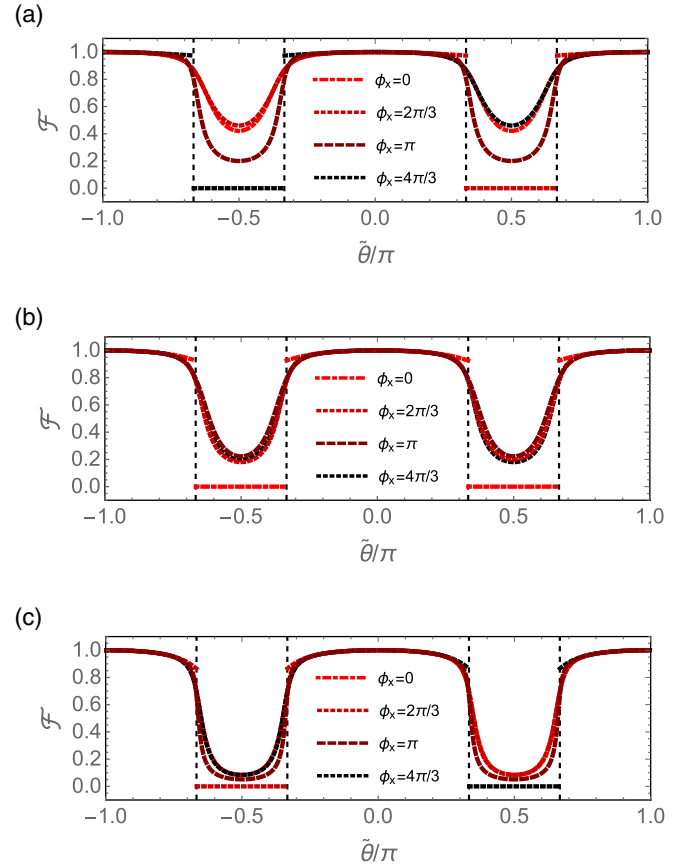

FIG. 7. The fidelity $\mathcal{F}$ of the Haldane model versus $\tilde{\theta}/\pi$ under twist boundary conditions with various ϕ. The vertical dashed lines guides the critical points $\tilde{\theta}_c/\pi = \pm 1/3, \pm 2/3$. (a) $L_x = 4$, $L_y = 4$. (b) $L_x = 6$, $L_y = 4$. (c) $L_x = 8$, $L_y = 4$. Here we take $t_1 = 1$, $M/t_2 = 4.5$, $\theta = 0$.
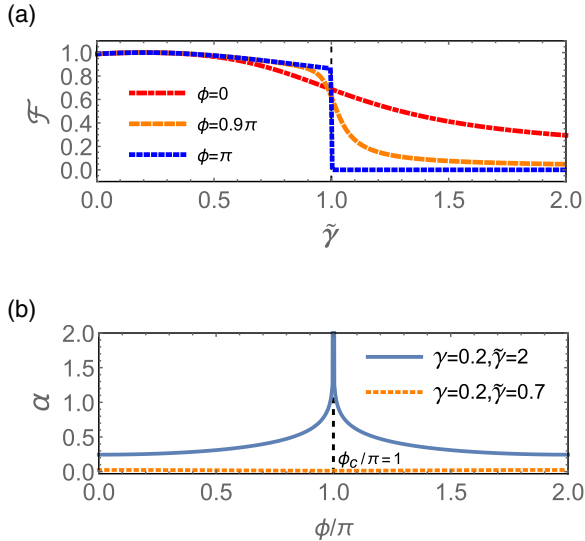
FIG. 8. (a) The fidelity $\mathcal{F}$ of the interacting SSH model versus $\tilde{\gamma}$ under twist boundary conditions with $\phi = 0$, 0.9π, and π. The vertical dashed line guides the critical point $\tilde{\gamma}_c = 1$. Here $\gamma = 0.2$. (b) The images of α versus ϕ/π. The solid blue line corresponds to $\gamma = 0.2$ and $\tilde{\gamma} = 2$, while the dotted orange line corresponds to $\gamma = 0.2$ and $\tilde{\gamma} = 0.7$. The vertical dashed line guides the divergent point $\phi_c/\pi = 1$. Here we take $L = 5$, $U = 0.1$.

the interacting SSH model. For large U, the system is in a density-wave phase, whereas for small U, there is still a phase transition through varying the parameter γ. We have obtained the approximate value of the phase transition point $\gamma_c \approx 1.038$ for $U = 0.1$ through the finite-size-scaling analysis of the fidelity. The numerical result suggests that the transition point is close to $\gamma = 1$.

We numerically calculate the fidelity $F(\gamma, \tilde{\gamma})$ versus $\tilde{\gamma}$ via exact diagonalization of a system with $L = 5$ by fixing $\gamma = 0.2$ for $U = 0.1$ under the twist boundary condition $c^{\dagger}_{L+1,A(B)} = c^{\dagger}_{1,A(B)} e^{i\phi}$ with various flux ϕ. Our numerical results are displayed in Fig. 8. In Fig. 8(a), for $\gamma = 0.2$, we find that the fidelity abruptly drops to zero at $\tilde{\gamma} = 1$ only under the antiperiodic boundary condition ($\phi = \pi$), suggesting that the phase transition point is given by $\gamma_c = 1$ for $U = 0.1$. In contrast, no sharp drop occurs and no exact zero of fidelity can be obtained for other ϕ. In Fig. 8(b), the images of α demonstrate that $\phi_c = \pi$ when $\tilde{\gamma}$ and γ belong to different phases. Our numerical results indicate that exact zeros of the fidelity obtained via the tuning of ϕ can provide a clear signature of the quantum phase transition even by studying a small size system of interacting SSH model.

III. SUMMARY AND DISCUSSION

In summary, we proposed a theoretical scheme for detecting quantum phase transition by seeking exact zeros of fidelity of finite-size systems with twist boundary conditions.

By considering the SSH model, the Creutz model and Haldane model as concrete examples, we demonstrated that exact zeros of fidelity of finite-size systems can be always accessed for $\tilde{\gamma}$ and γ in different phases under a proper twist boundary condition, whereas no exact zero exists for $\tilde{\gamma}$ and γ in the same phase. Consequently, we can observe a discontinued behavior of fidelity at the phase transition point by tuning the twist flux parameter ϕ. Changing ϕ continuously, we unveiled that the decay rate function α of the fidelity is divergent at the critical magnetic flux ϕ_c for $\tilde{\gamma}$ and γ in different phases, while α is smooth everywhere for $\tilde{\gamma}$ and γ in the same phase. We also exhibited the applicability of our theoretical scheme to the interacting SSH model.

Our work provides an efficient way for detecting quantum phase transition by studying small-size systems via the introduction of an additional magnetic flux. A natural question concerns whether such a scheme is applicable to a general context of models with quantum phase transitions, including correlated systems, the Ising model with finite/infinite interaction range, and models without a spatial lattice interpretation, e.g., the Lipkin-Meshkov-Glick model [38,39]. Although we show the applicability of our theoretical scheme to the interacting SSH model in Sec. II D, our scheme does not always work for general correlated systems and models without spatial interpretation, for which the momentum is even not well defined. In the present work, the gap between the first excited state and ground state is a function of momentum for all the studied models, and thus we can tune the gap to approach zero by tuning the magnetic flux properly. For systems without spatial interpretation, the gap of a finite-size system is not necessary to be a function of momentum, and thus our scheme is not necessary to be applicable to these systems.

Our scheme also suggests an alternative way for experimentally detecting signature of QPT in finite-size quantum systems, which, however, relies on the ability of creating tunable magnetic flux in quantum simulators. For the experimental setup in a trapped-ion quantum simulator [40,41], it is still a great challenge to create tunable magnetic flux in the setup. However, it seems that cold atomic system is a promising platform for producing tunable magnetic flux. By using multifrequency Bragg lasers, the SSH model on a momentum lattice was experimentally realized [42], where the synthetic magnetic flux through the ring are tunable [43]. Thus we expect it to be a promising platform to observe signature of QPT by using the theoretical scheme proposed in this work.

[1] S. Sachdev, *Quantum Phase Transitions* (Cambridge University Press, Cambridge, UK, 1999).

[2] P. Zanardi and N. Paunković, Ground state overlap and quantum phase transitions, Phys. Rev. E **74**, 031123 (2006).

[3] W. L. You, Y. W. Li, and S. J. Gu, Fidelity, dynamic structure factor, and susceptibility in critical phenomena, Phys. Rev. E **76**, 022101 (2007).

[4] L. C. Venuti and P. Zanardi, Quantum critical scaling of the geometric tensors, Phys. Rev. Lett. **99**, 095701 (2007).

[5] P. Zanardi, P. Giorda, and M. Cozzini, Information-theoretic differential geometry of quantum phase transitions, Phys. Rev. Lett. **99**, 100603 (2007).

[6] H. T. Quan, Z. Song, X. F. Liu, P. Zanardi, and C. P. Sun, Decay of Loschmidt echo enhanced by quantum criticality, Phys. Rev. Lett. **96**, 140604 (2006).

[7] S. Chen, L. Wang, Y. Hao, and Y. Wang, Intrinsic relation between ground-state fidelity and the characterization of a quantum phase transition, Phys. Rev. A **77**, 032111 (2008).

[8] H.-Q. Zhou, J.-H. Zhao, and B. Li, Fidelity approach to quantum phase transitions: Finite-size scaling for the quantum Ising model in a transverse field, J. Phys. A **41**, 492002 (2008).

[9] P. Buonsante and A. Vezzani, Ground-state fidelity and bipartite entanglement in the Bose-Hubbard model, Phys. Rev. Lett. **98**, 110601 (2007).

[10] M.-F. Yang, Ground-state fidelity in one-dimensional gapless models, Phys. Rev. B **76**, 180403(R) (2007).

[11] S. Chen, L. Wang, S. J. Gu, and Y. Wang, Fidelity and quantum phase transition for the Heisenberg chain with next-nearest-neighbor interaction, Phys. Rev. E **76**, 061108 (2007).

[12] S. J. Gu, H.-M. Kwok, W.-Q. Ning, and H.-Q. Lin, Fidelity susceptibility, scaling, and universality in quantum critical phenomena, Phys. Rev. B **77**, 245109 (2008).

[13] M. M. Rams and B. Damski, Quantum fidelity in the thermodynamic limit, Phys. Rev. Lett. **106**, 055701 (2011).

[14] V. Mukherjee, A. Polkovnikov, and A. Dutta, Oscillating fidelity susceptibility near a quantum multicritical point, Phys. Rev. B **83**, 075118 (2011).

[15] G. Sun, A. K. Kolezhuk, and T. Vekua, Fidelity at Berezinskii-Kosterlitz-Thouless quantum phase transitions, Phys. Rev. B **91**, 014418 (2015).

[16] E. J. König, A. Levchenko, and N. Sedlmayr, Universal fidelity near quantum and topological phase transitions in finite one-dimensional systems, Phys. Rev. B **93**, 235160 (2016).

[17] Q. Luo, J. Zhao, and X. Wang, Fidelity susceptibility of the anisotropic XY model: The exact solution, Phys. Rev. E **98**, 022106 (2018).

[18] G. Sun, B.-B. Wei, and S.-P. Kou, Fidelity as a probe for a deconfined quantum critical point, Phys. Rev. B **100**, 064427 (2019).

[19] M. Heyl, A. Polkovnikov, and S. Kehrein, Dynamical quantum phase transitions in the transverse-field Ising model, Phys. Rev. Lett. **110**, 135704 (2013).

[20] S. Vajna and B. Dóra, Topological classification of dynamical phase transitions, Phys. Rev. B **91**, 155127 (2015).

[21] J. C. Budich and M. Heyl, Dynamical topological order parameters far from equilibrium, Phys. Rev. B **93**, 085416 (2016).

[22] C. Karrasch and D. Schuricht, Dynamical phase transitions after quenches in nonintegrable models, Phys. Rev. B **87**, 195104 (2013).

[23] M. Heyl, Scaling and universality at dynamical quantum phase transitions, Phys. Rev. Lett. **115**, 140602 (2015).

[24] C. Yang, L. Li, and S. Chen, Dynamical topological invariant after a quantum quench, Phys. Rev. B **97**, 060304(R) (2018).

[25] M. Heyl, Dynamical quantum phase transitions: A review, Rep. Prog. Phys. **81**, 054001 (2018).

[26] D. Liska and V. Gritsev, The Loschmidt index, SciPost Phys. **10**, 100 (2021).

[27] B. Zhou, Y. Zeng, and S. Chen, Exact zeros of the Loschmidt echo and quantum speed limit time for the dynamical quantum phase transition in finite-size systems, Phys. Rev. B **104**, 094311 (2021).

[28] Y. Zeng, B. Zhou, and S. Chen, Dynamical singularity of the rate function for quench dynamics in finite-size quantum systems, Phys. Rev. B **107**, 134302 (2023).

[29] Z.-R. Zhu, B. Shao, J. Zou, and L.-A. Wu, Orthogonality catastrophe and quantum speed limit for dynamical quantum phase transition, Physica A **634**, 129455 (2024).

[30] P. W. Anderson, Infrared catastrophe in Fermi gases with local scattering potentials, Phys. Rev. Lett. **18**, 1049 (1967).

[31] W. P. Su, J. R. Schrieffer, and A. J. Heeger, Solitons in polyacetylene, Phys. Rev. Lett. **42**, 1698 (1979).

[32] L. Li, Z. Xu, and S. Chen, Topological phases of generalized Su-Schrieffer-Heeger models, Phys. Rev. B **89**, 085111 (2014).

[33] The oblique line in the Fig. 1(b) is fitted by $\alpha = c - \ln 2/L$, which gives the lower bound of the α and can be derived by analytically calculating the difference of the integral and the summation $-\frac{1}{2\pi} \int \ln \mathcal{F}_k dk - (-\frac{1}{L} \sum_k \ln \mathcal{F}_k)$. For $\tilde{\gamma}$ and γ in the same phase, $\ln \mathcal{F}_k$ is a smooth function of k, and $-\frac{1}{2\pi} \int \ln \mathcal{F}_k dk - (-\frac{1}{L} \sum_k \ln \mathcal{F}_k) \ll 1/L$. For $\tilde{\gamma}$ and γ in different phases, if the fidelity has a k_c mode which is exactly situated in the middle of two quantized momentum k modes, i.e., $\min |k - k_c| = \pi/L$, then $-\frac{1}{2\pi} \int_0^{k_c - \pi/L} \ln \mathcal{F}_k dk - \frac{1}{2\pi} \int_{k_c + \pi/L}^{2\pi} \ln \mathcal{F}_k dk - (-\frac{1}{L} \sum_{k \neq k_c - \pi/L} \ln \mathcal{F}_k) \ll 1/L$ and $-\frac{1}{2\pi} \int_{k_c - \pi/L}^{k_c + \pi/L} \ln \mathcal{F}_k dk - (-\frac{1}{L} \ln \mathcal{F}_{k_c - \pi/L}) \approx \ln 2/L$. Adding them up, we get $-\frac{1}{2\pi} \int_0^{2\pi} \ln \mathcal{F}_k dk - (-\frac{1}{L} \sum_k \ln \mathcal{F}_k) \approx \ln 2/L$. As a result, we get $\alpha(L) \approx \alpha_\infty - \ln 2/L$, here α_∞ is the value of α in the thermodynamic limit. If the fidelity has a k_c mode satisfises $\min |k - k_c| < \pi/L$, then $\alpha(L) > \alpha_\infty - \ln 2/L$. The above is the case with the fidelity having only one k_c mode. For the case with the fidelity having n k_c modes, the slope of the lower bound is $-n \ln 2$.

[34] M. Creutz, End states, ladder compounds, and domain-wall fermions, Phys. Rev. Lett. **83**, 2636 (1999).

[35] R. Jafari, H. Johannesson, A. Langari, and M. A. Martin-Delgado, Quench dynamics and zero-energy modes: The case of the Creutz model, Phys. Rev. B **99**, 054302 (2019).

[36] F. D. M. Haldane, Model for a quantum Hall effect without Landau levels: Condensed-matter realization of the "parity anomaly," Phys. Rev. Lett. **61**, 2015 (1988).

[37] H.-K. Tang, M. A. Marashli, and W. C. Yu, Unveiling quantum phase transitions by fidelity mapping, Phys. Rev. B **104**, 075142 (2021).

[38] H. J. Lipkin, N. Meshkov, and A. J. Glick, Validity of many-body approximation methods for a solvable model: (I). Exact solutions and perturbation theory, Nucl. Phys. **62**, 188 (1965).

[39] J. Ma, X. Wang, and S. Gu, Many-body reduced fidelity susceptibility in Lipkin-Meshkov-Glick model, Phys. Rev. E **80**, 021124 (2009).

[40] P. Jurcevic, H. Shen, P. Hauke, C. Maier, T. Brydges, C. Hempel, B. P. Lanyon, M. Heyl, R. Blatt, and C. F. Roos, Direct observation of dynamical quantum phase transitions in

an interacting many-body system, Phys. Rev. Lett. **119**, 080501 (2017).

[41] J. Zhang, G. Pagano, P. W. Hess, A. Kyprianidis, P. Becker, H. Kaplan, A. V. Gorshkov, Z.-X. Gong, and C. Monroe, Observation of a many-body dynamical phase transition with a 53-qubit quantum simulator, Nature (London) **551**, 601 (2017).

[42] D. Xie, W. Gou, T. Xiao, B. Gadway and B. Yan, Topological characterizations of an extended Su-Schrieffer-Heeger model, Npj Quant. Inf. **5**, 55 (2019).

[43] W. Gou, T. Chen, D. Xie, T. Xiao, T.-S. Deng, B. Gadway, W. Yi, and B. Yan, Tunable nonreciprocal quantum transport through a dissipative Aharonov-Bohm ring in ultracold atoms, Phys. Rev. Lett. **124**, 070402 (2020).